Supplementary Material

for

Mechanism of antiradical activity of coumarin-trihydroxybenzohydrazide derivatives: A comprehensive kinetic DFT study

Žiko Milanović [1], Dušan Dimić [2], Edina H. Avdović [1], Dušica M. Simijonović [1], Đura Nakarada [2], Vladimir Jakovljević [3], and Radiša Vojinović [3,*], Zoran S. Marković [1,4]

[1]*University of Kragujevac, Institute for Information Technologies, Department of Science, Liceja Kneževine Srbije 1A, 34000 Kragujevac, Serbia;*

[2]*University of Belgrade, Faculty of Physical Chemistry, Studentski trg 12-16, 11000 Belgrade, Serbia;*

[3]*University of Kragujevac, Faculty of Medical Sciences, Svetozara Markovića 69, 34000 Kragujevc, Republic of Serbia;*

[4]*State University of Novi Pazar, Department of Natural Science and Mathematics, Vuka Karadžića bb, 36300, Novi Pazar, Serbia, Serbia;*

**Correspondence: rhvojinovic@medf.kg.ac.rs; Tel.: +381 34 306 800*

To quantify the molar fractions of acid-base species, the relationship between the acid constants (*Ka*) and the *p*K$_a$ values as well as the expression for the equilibrium constant of the deprotonation process was used:

$$Ka_1 = 10^{-pKa1} \tag{1s}$$

$$Ka_2 = 10^{-pKa2} \tag{2s}$$

$$Ka_3 = 10^{-pKa3} \tag{3s}$$

$$Ka_4 = 10^{-pKa4} \tag{4s}$$

$$Ka_1 = \frac{\left[H_3A^-\right]\left[H^+\right]}{\left[H_4A\right]} \tag{5s}$$

$$Ka_2 = \frac{\left[H_2A^{2-}\right]\left[H^+\right]}{\left[H_3A^-\right]} \tag{6s}$$

$$Ka_3 = \frac{\left[HA^{3-}\right]\left[H^+\right]}{\left[H_2A^{2-}\right]} \tag{7s}$$

$$Ka_4 = \frac{\left[A^{4-}\right]\left[H^+\right]}{\left[HA^{3-}\right]} \tag{8s}$$

Molar fractions (*f*) of the represented acid-base species, were calculated using the following equations:

$$f(A^{4-}) = \frac{1}{1+\beta_1\left[H^+\right]+\beta_2\left[H^+\right]^2+\beta_2\left[H^+\right]^2+\beta_4\left[H^+\right]^4} \tag{9s}$$

$$f(HA^{3-}) = \beta_1 \left[H^+ \right] f(A^{4-}) \quad (10s)$$

$$f(H_2A^{2-}) = \beta_2 \left[H^+ \right]^2 f(HA^{3-}) \quad (11s)$$

$$f(H_3A^{-}) = \beta_3 \left[H^+ \right]^3 f(H_2A^{2-}) \quad (12s)$$

where $[H^+]$ represents the concentration of hydrogen ions at physiological pH in this case ($[H^+]=3.98\times10^{-8}$ M), while β represents global formation equilibrium constants:

$$\beta_1 = 10^{pKa4} \quad (13s)$$

$$\beta_2 = 10^{pKa4+pKa3} \quad (14s)$$

$$\beta_3 = 10^{pKa4+pKa3+pKa2} \quad (15s)$$

$$\beta_4 = 10^{pKa4+pKa3+pKa2+pKa1} \quad (16s)$$

The overall rate constants ($k_{overall}$) for the reactions between the investigated compounds and $HO^{\bullet}$ were calculated by the following equations:

$$k_{overall} = f(H_4A)\times k_{TOT}^{H_4A} + f(H_3A^{-})\times k_{TOT}^{H_3A^{-}} + f(H_2A^{2-})\times k_{TOT}^{H_2A^{2-}} + f(HA^{3-})\times k_{TOT}^{HA^{3-}} + f(A^{4-})\times k_{TOT}^{A^{4-}} \quad (17s)$$

Due to the very small proportion of acid-base species at physiological pH, eq. 17s can be represented as:

$$k_{overall}^{Comp1} = f(H_4A) \times k_{TOT}^{H_4A} + f(H_3A^-) \times k_{TOT}^{H_3A^-} + f(H_2A^{2-}) \times k_{TOT}^{H_2A^{2-}} \quad (18s)$$

$$k_{overall}^{Comp2} = f(H_4A) \times k_{TOT}^{H_4A} + f(H_3A^-) \times k_{TOT}^{H_3A^-} \quad (19s)$$

where k_{TOT} represent the sum of the favorable reaction pathways for the investigation species and HO•:

$$k_{TOT} = k_{HAT} + k_{RAF} + k_{SPL} + k_{ET} \quad (20s)$$

Antioxidative capacity r^T of the examined antioxidant relative to trolox (**Tx**)/gallic acid (**GA**) ($k_{overall}^{Ref}$) was calculated using the formula:

$$r^T = \frac{k_{overall}}{k_{overall}^{Ref}} \quad (21s)$$

The relative amounts of products (%), i.e. branching ratios (Γi) were determined:

$$\Gamma_i = \frac{k_i}{k_{overall}} \quad (22s)$$

to evaluate which of the mechanistic pathways, i, is dominant.

Standard mechanisms of antioxidant action between neutral forms of the investigated compounds and HO• radical:

HAT/PCET: $H_4A + HO^\bullet \rightarrow H_3A^\bullet + H_2O$ (23s)

RAF: $H_4A + HO^\bullet \rightarrow [H_4A\text{-}OH]^\bullet$ (24s)

SET: $H_4A + HO^{\bullet} \rightarrow H_4A^{\bullet+} + HO^{-}$ (25s)

PT: $H_4A^{\bullet+} + HO^{-} \rightarrow H_3A^{\bullet} + H_2O$ (26s)

SPL: $H_4A + HO^{-} \rightarrow H_3A^{-} + H_2O$ (27s)

ET: $H_3A^{-} + HO^{\bullet} \rightarrow H_3A^{\bullet} + HO^{-}$ (28s)

where H_4A, $H_3A^{\bullet}$, $[HO\text{-}H_4A]^{\bullet}$, $H_4A^{\bullet+}$, and H_3A^{-} denote neutral species, its radical, radical adduct, radical cation, and anion.

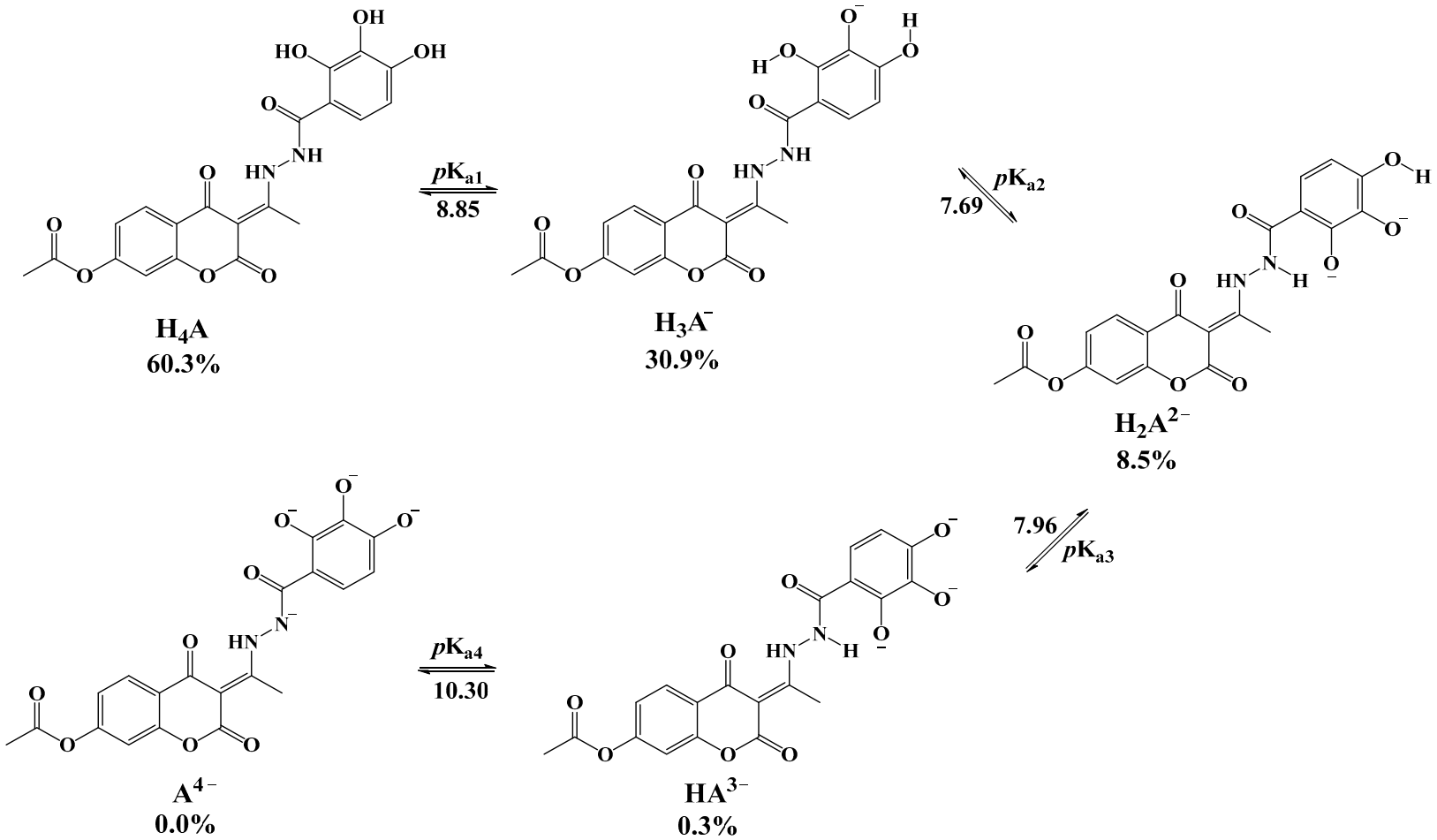

Figure S1. Deprotonation route, estimated pK_a values and molar fractions of acid-base species of **1** at physiological pH (7.4)

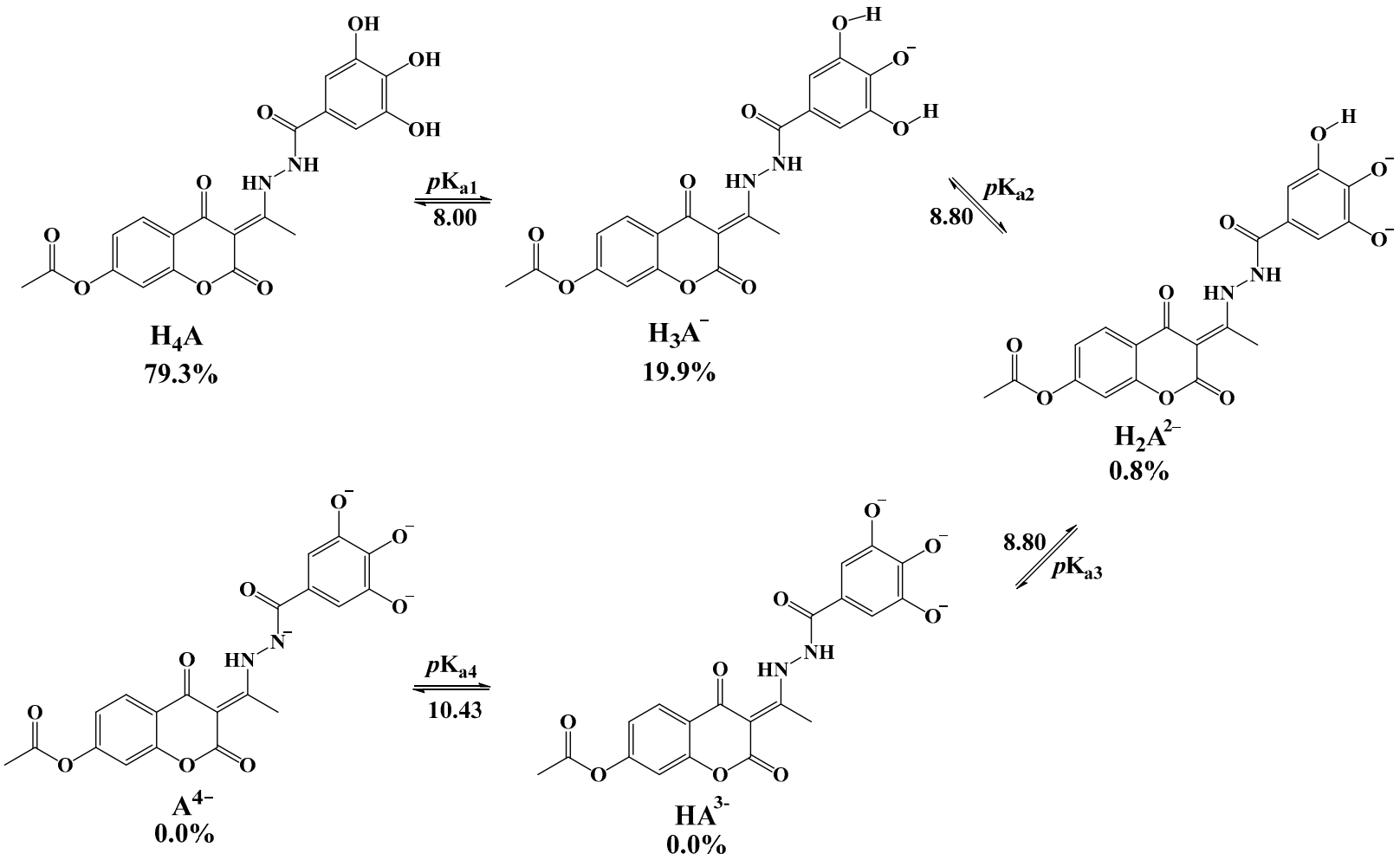

Figure S2. Deprotonation route, estimated pKa values and molar fractions of acid-base species of **2** at physiological pH (7.4)

Table S1. 2D geometries of the investigated acid-base species of **1** compound that participate in the various investigated mechanisms of antiradical action. The black color describes the thermodynamically favored products obtained between neutral species **H_4A** and $HO^{\bullet}$. The red color describes the favored products obtained between monoanionic species **H_3A^-**(**$H_3A^{\bullet}$**) and $HO^{\bullet}$, while the blue color describes favored products obtained between dianionic species **H_2A^{2-}**(**$H_2A^{\bullet-}$**) and $HO^{\bullet}$.

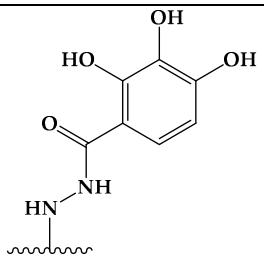			
H_4A			
SPLET (H_4A)			
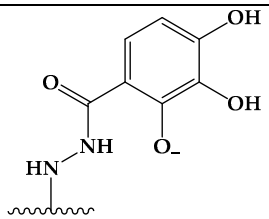	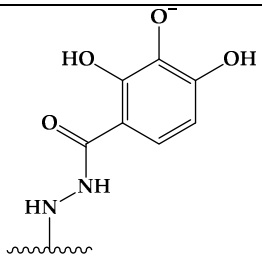	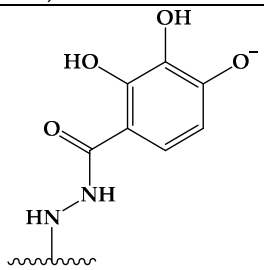	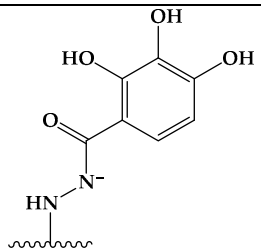
2″-OH	3″-OH	4″-OH	N2-H
HAT/PCET (H_4A)			
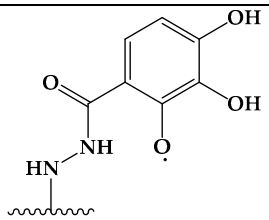	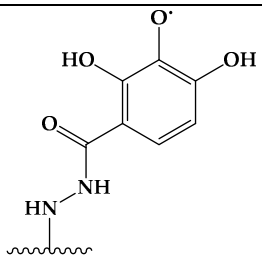	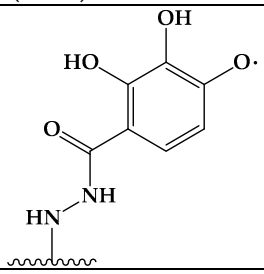	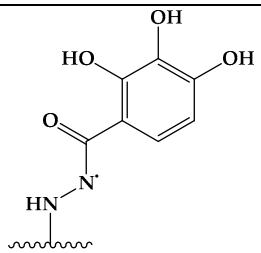
2″-OH	3″-OH	4″-OH	N2-H
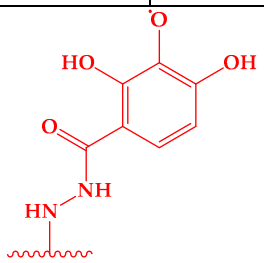			

$H_3A^{\bullet}$/ H_3A^{-}		
HAT/PCET ($H_3A^{\bullet}$/ H_3A^{-})		
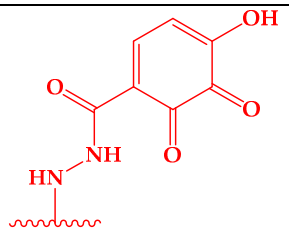	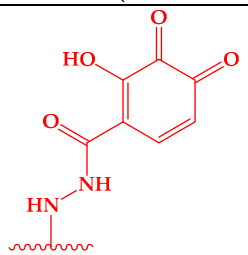	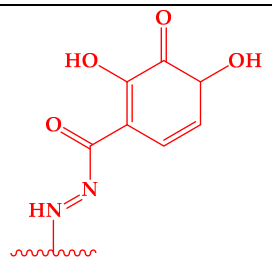
2″-OH	4″-OH	N2-H
PT ($H_3A^{\bullet}$/ H_3A^{-})		
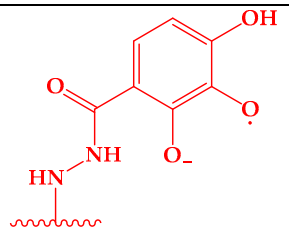	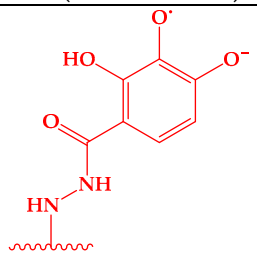	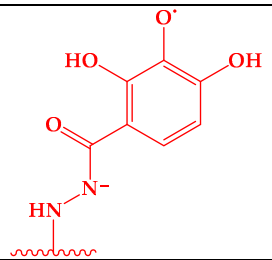
2″-OH	4″-OH	N2-H
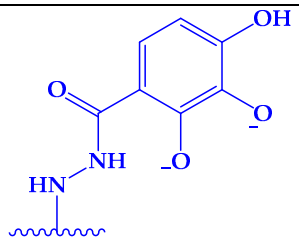 H_2A^{2-}/ $H_2A^{\bullet-}$		
HAT/PCET (H_2A^{2-}/ $H_2A^{\bullet-}$)		
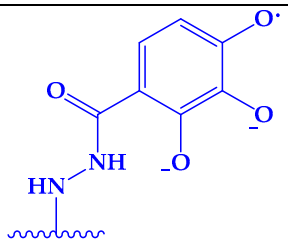	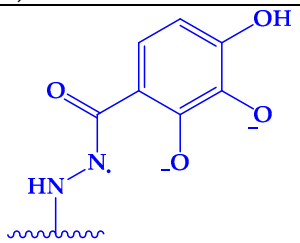	
4″-OH	2-NH/2″-OH	
PT (H_2A^{2-}/ $H_2A^{\bullet-}$)		

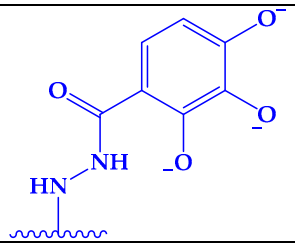	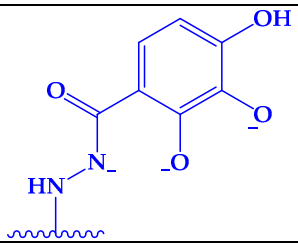

Table S2. 2D geometries of the investigated acid-base species of compound **2** that participate in the various investigated mechanisms of antiradical action. The black color describes the thermodynamically favored products obtained between neutral species **H_4A** and $HO^{\bullet}$. The red color describes the favored products obtained between monoanionic species **H_3A^-**(**$H_3A^{\bullet}$**) and $HO^{\bullet}$.

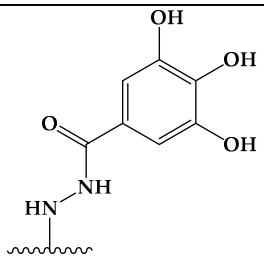 H_4A		
SPLET (H_4A)		
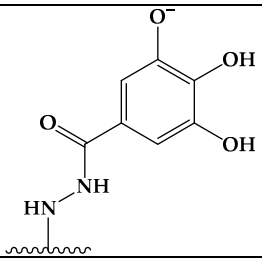	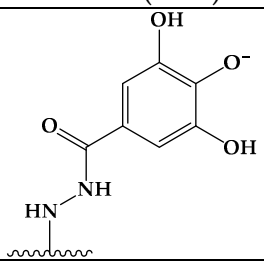	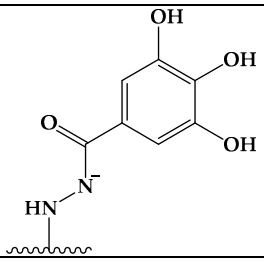
3″-OH/5″-OH	4″-OH	N2-H
HAT/PCET (H_4A)		
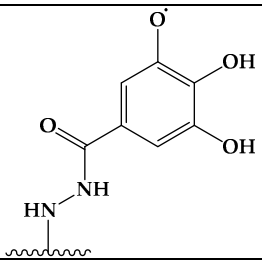	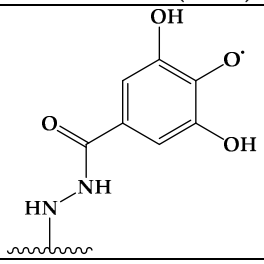	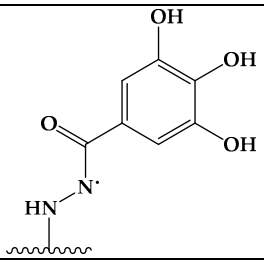

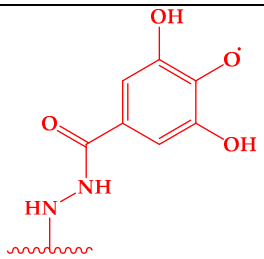 H_3A^-		
HAT/PCET ($H_3A^{\bullet}$/ H_3A^-)		
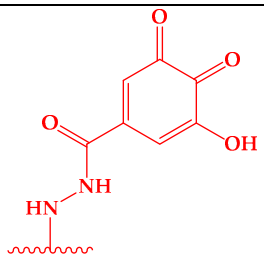	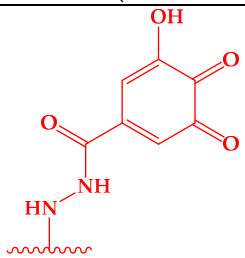	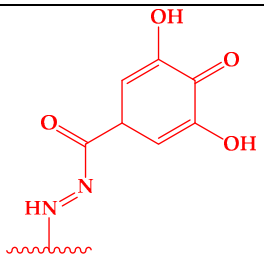
3″-OH	5″-OH	N2-H
PL ($H_3A^{\bullet}$/ H_3A^-)		
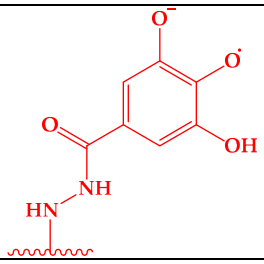	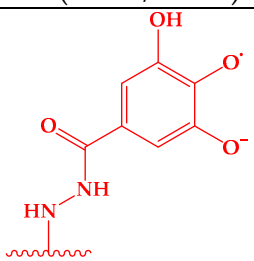	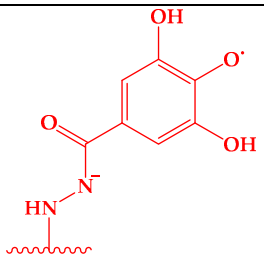
3″-OH	5″-OH	N2-H

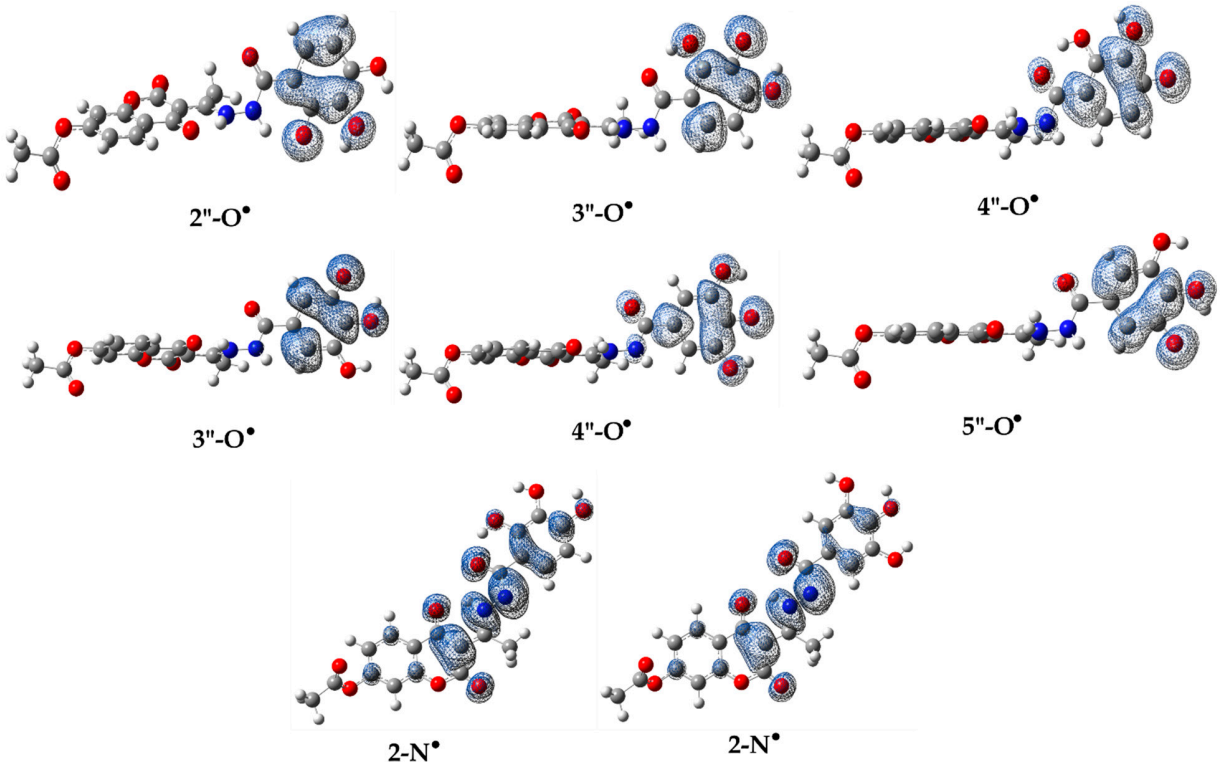

Figure S3. Spin density distribution maps (0.002 electrons/bohr^3) of formed radical species formed in the reaction between **H_4A** of compounds **1** (a,c) and **2** (b,d) and HO• radical. Blue color represents positive spin density values.

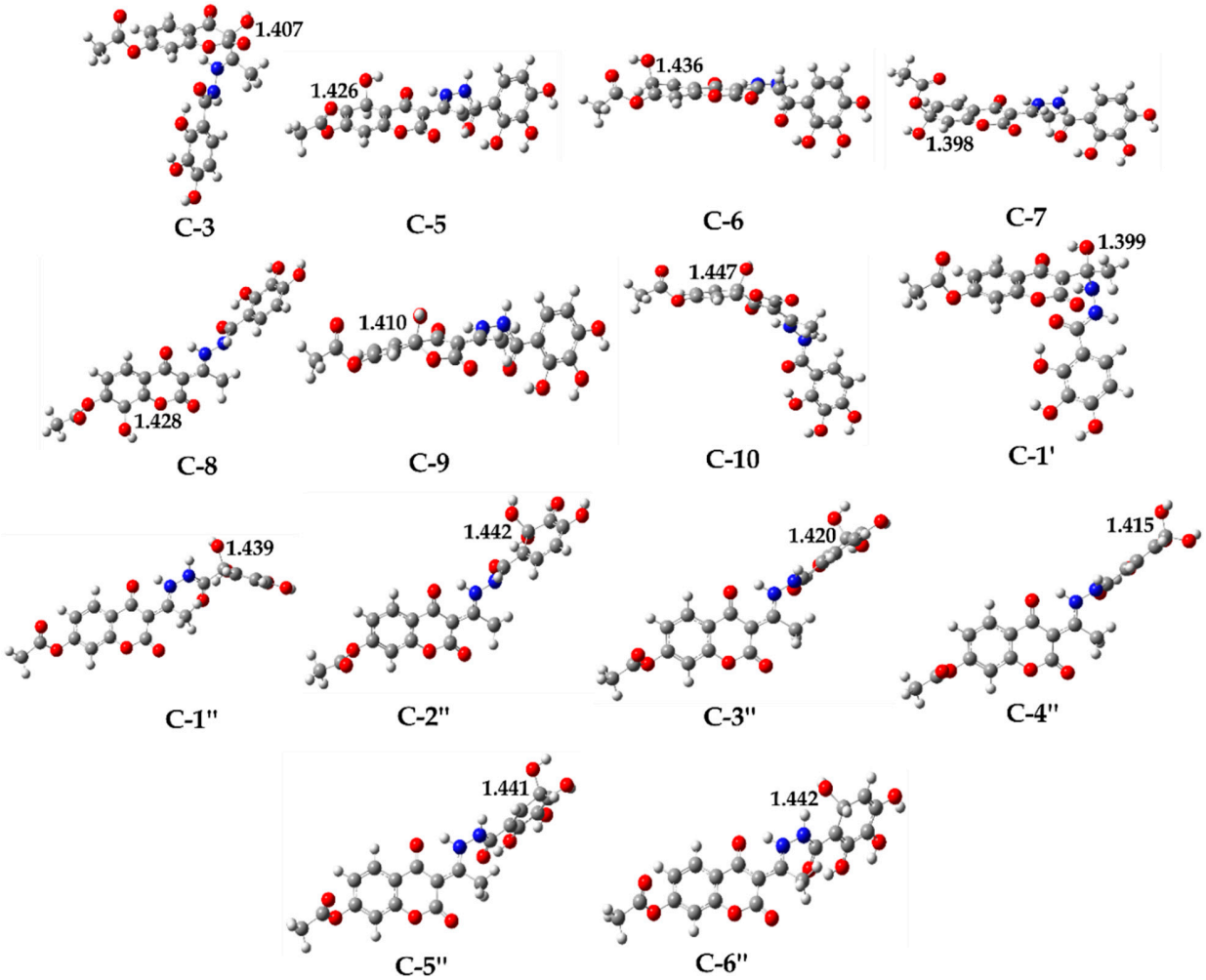

Figure S4. Optimized geometries of radical adducts with characteristic intramolecular distances (Å) formed between **H_4A** of compound **1** and HO•

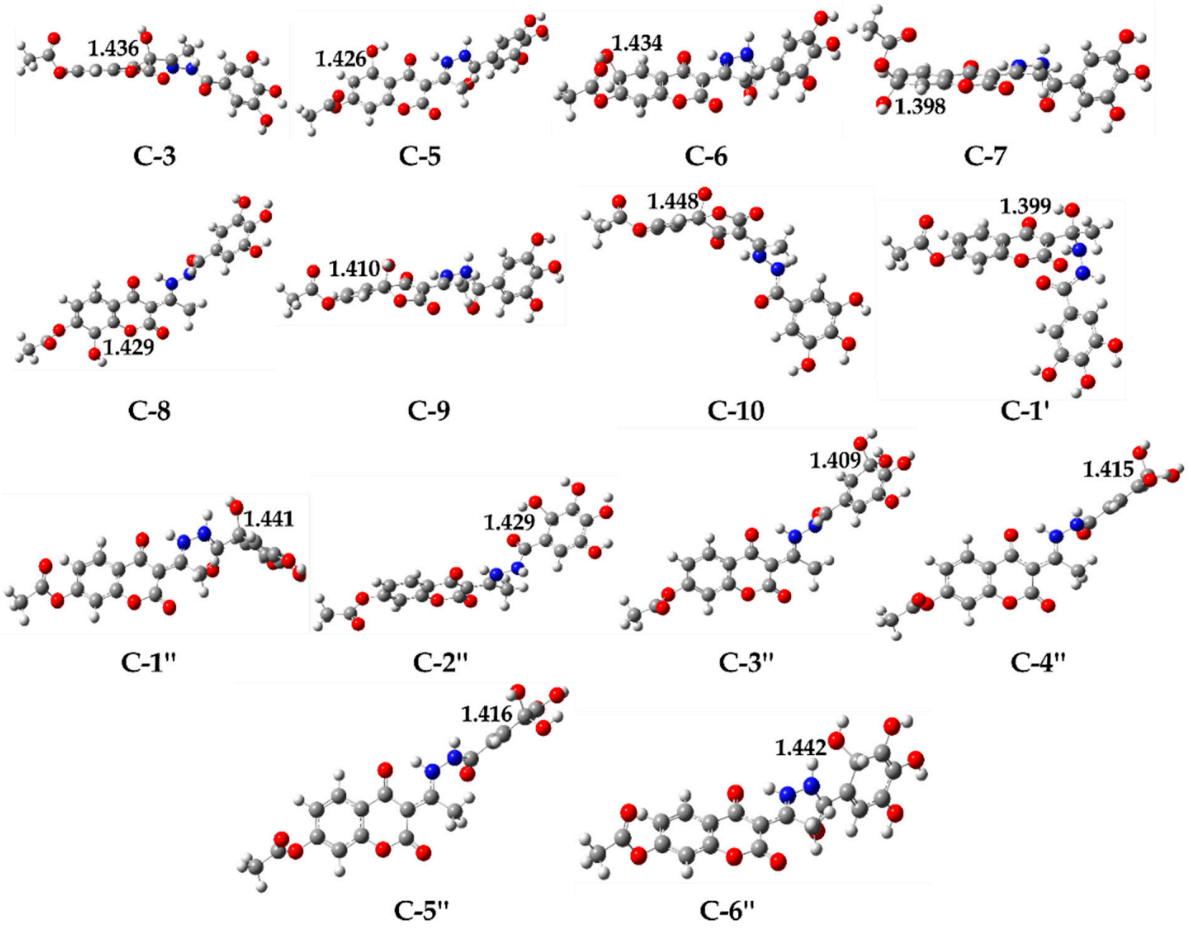

Figure S5. Optimized geometries of radical adducts with characteristic intramolecular distances (Å) formed between **H$_4$A** of compound **2** and HO$^{\bullet}$

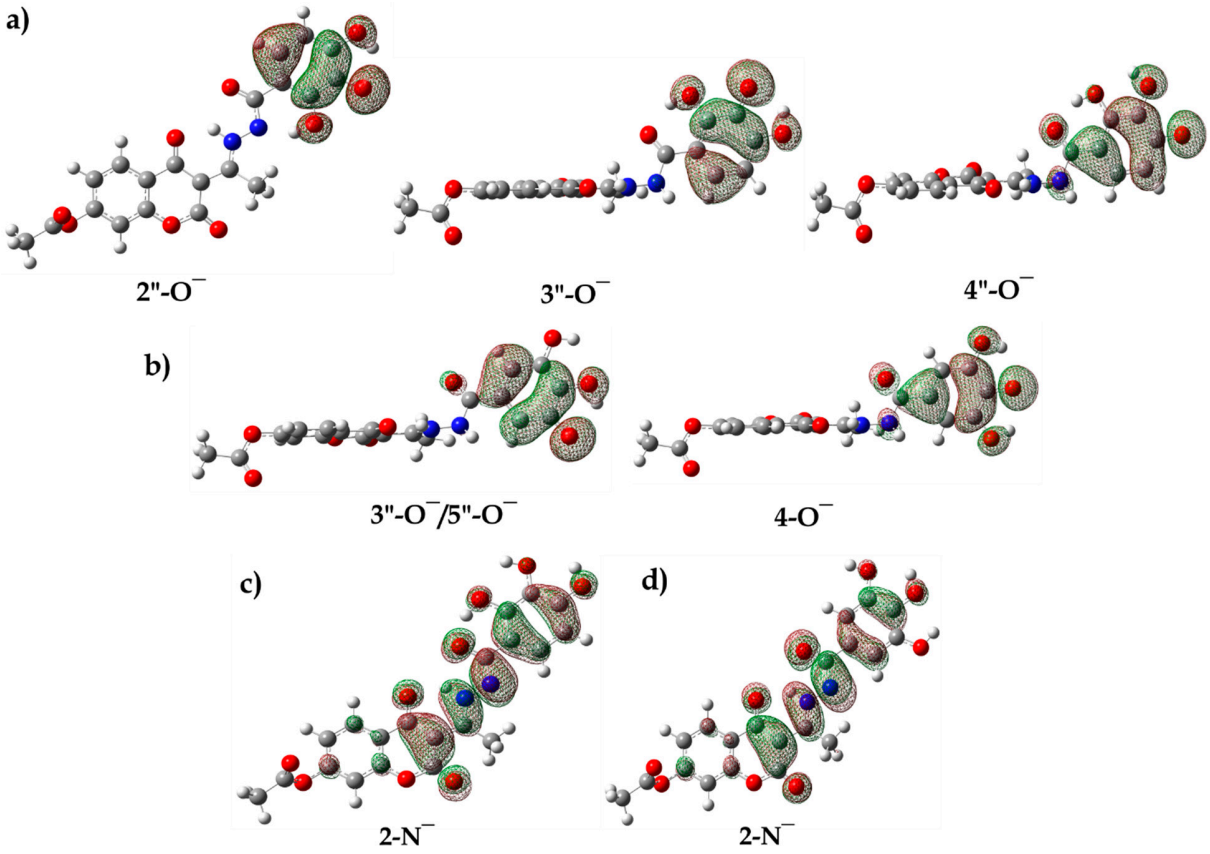

Figure S6. HOMO (*Highest Occupied Molecular Orbital*) orbitals of formed phenoxide anions formed in the reaction between **H_4A** of compounds **1** (a,c) and **2** (b,d) and HO^-

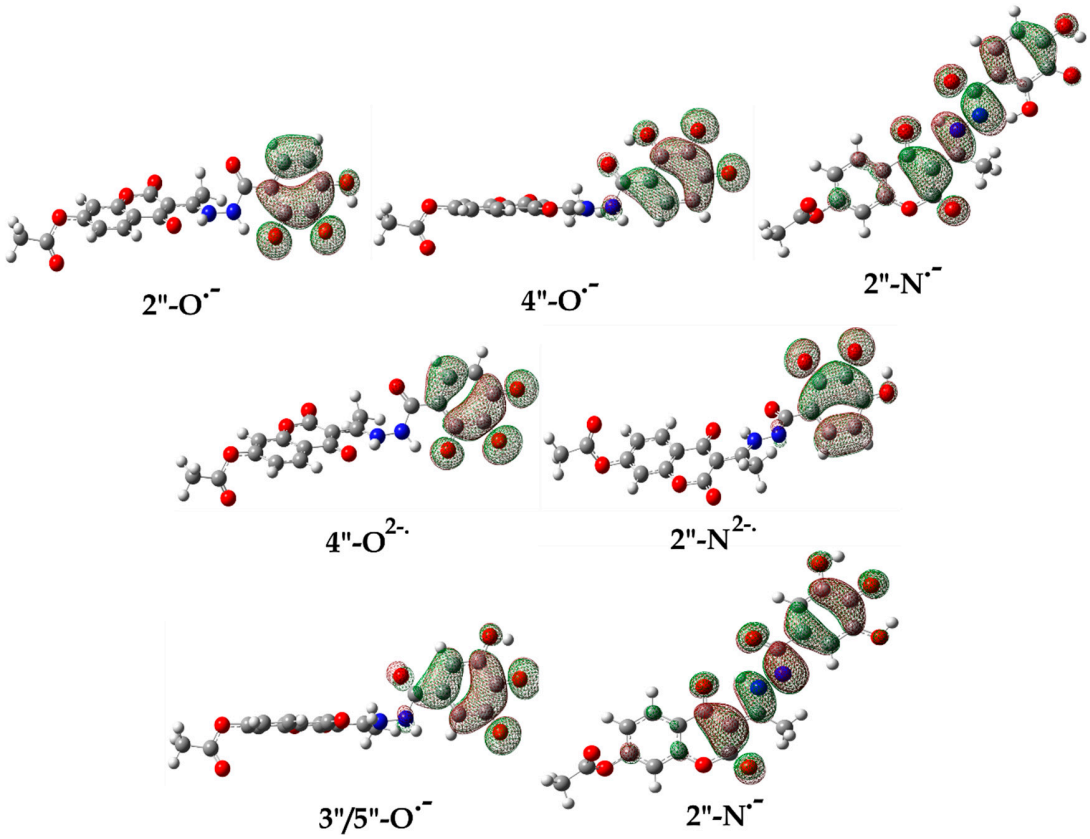

Figure S7. HOMO orbitals for the corresponding $\mathbf{H_2A^{\bullet-}}$ nad $\mathbf{H_2A^{2\bullet-}}$ species formed in the reaction of proton transfer from $\mathbf{H_3A^{\bullet}}$ (top) and $\mathbf{H_3A^{\bullet-}}$ (middle) of compound **1** to HO^- as well as from $\mathbf{H_3A^{\bullet}}$ of compound **2** (bottom) to HO^-.

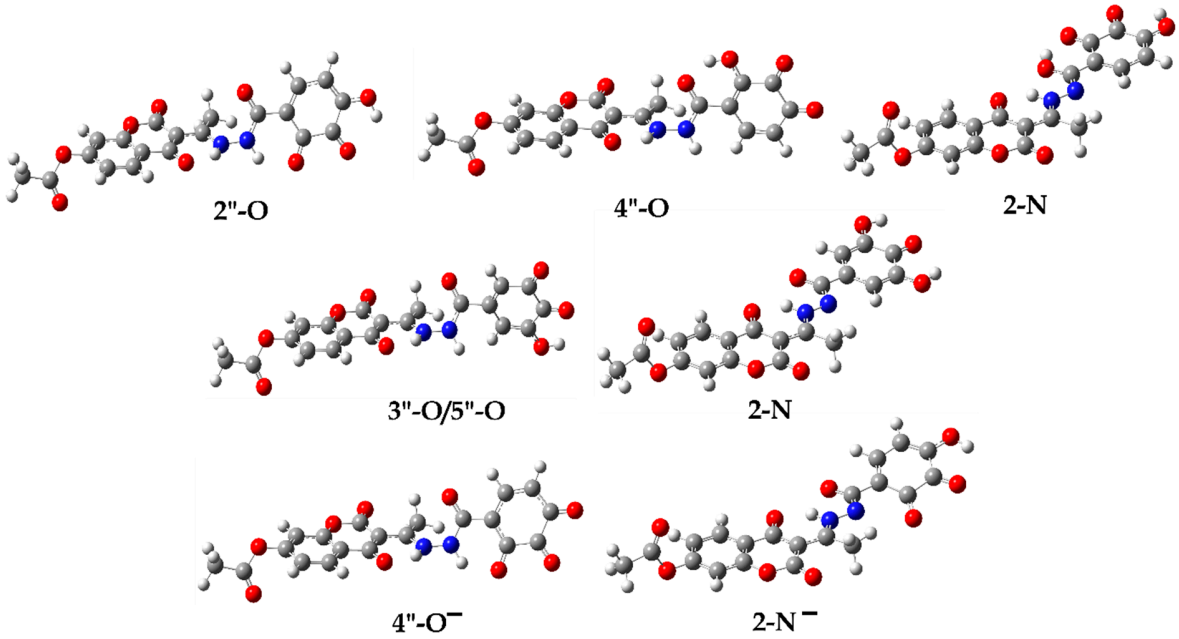

Figure S8. Optimized geometries of neutral **H_2A** products of compounds **1** (top) and **2** (middle) and monoanionic **HA^-** product (bottom) formed in the reaction between **$H_3A^\bullet$** and **$H_2A^{\bullet-}$** and $HO^\bullet$.

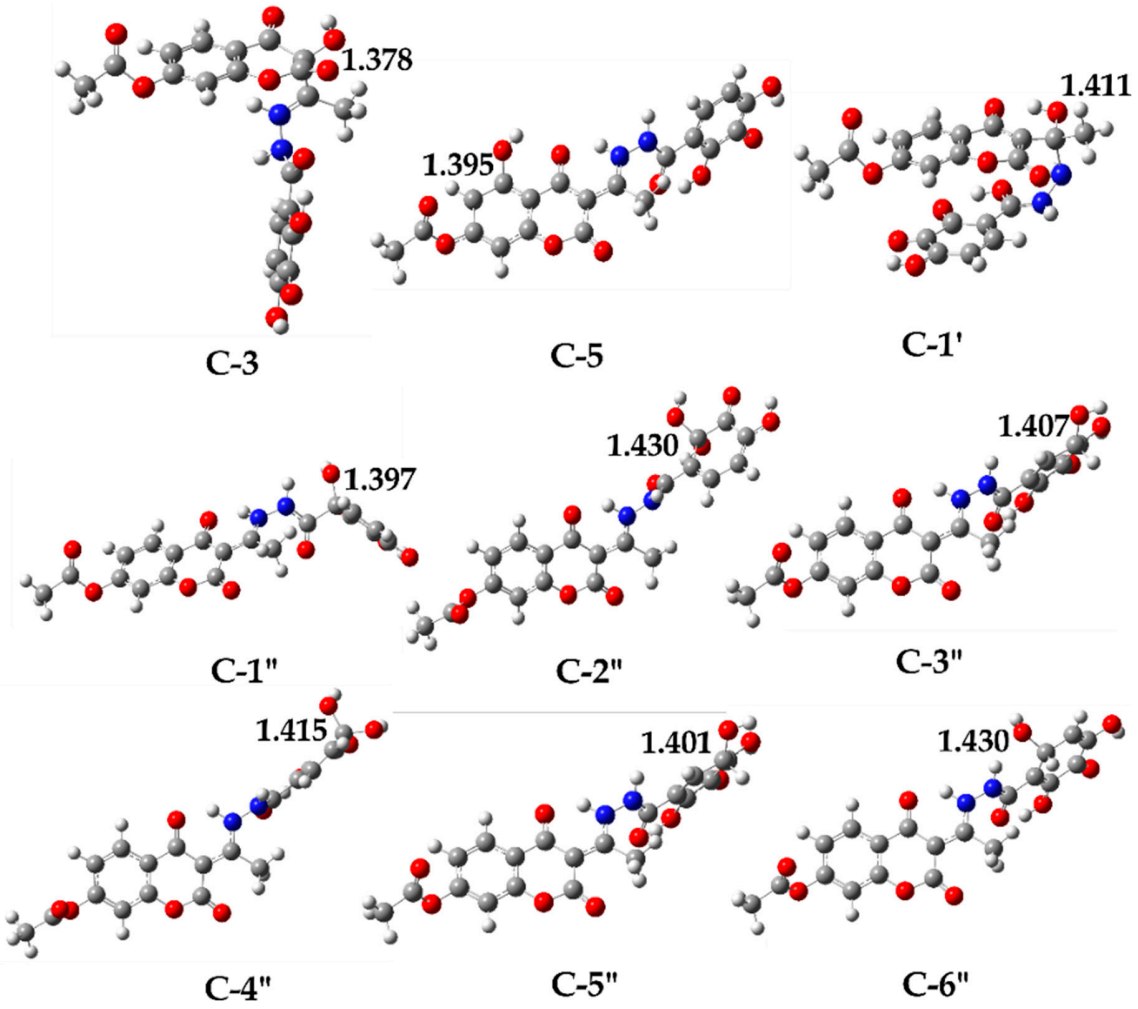

Figure S9. Optimized geometries of adducts with characteristic intramolecular distances (Å) formed between $\mathbf{H_3A^{\bullet}}$ of compound **1** and $HO^{\bullet}$

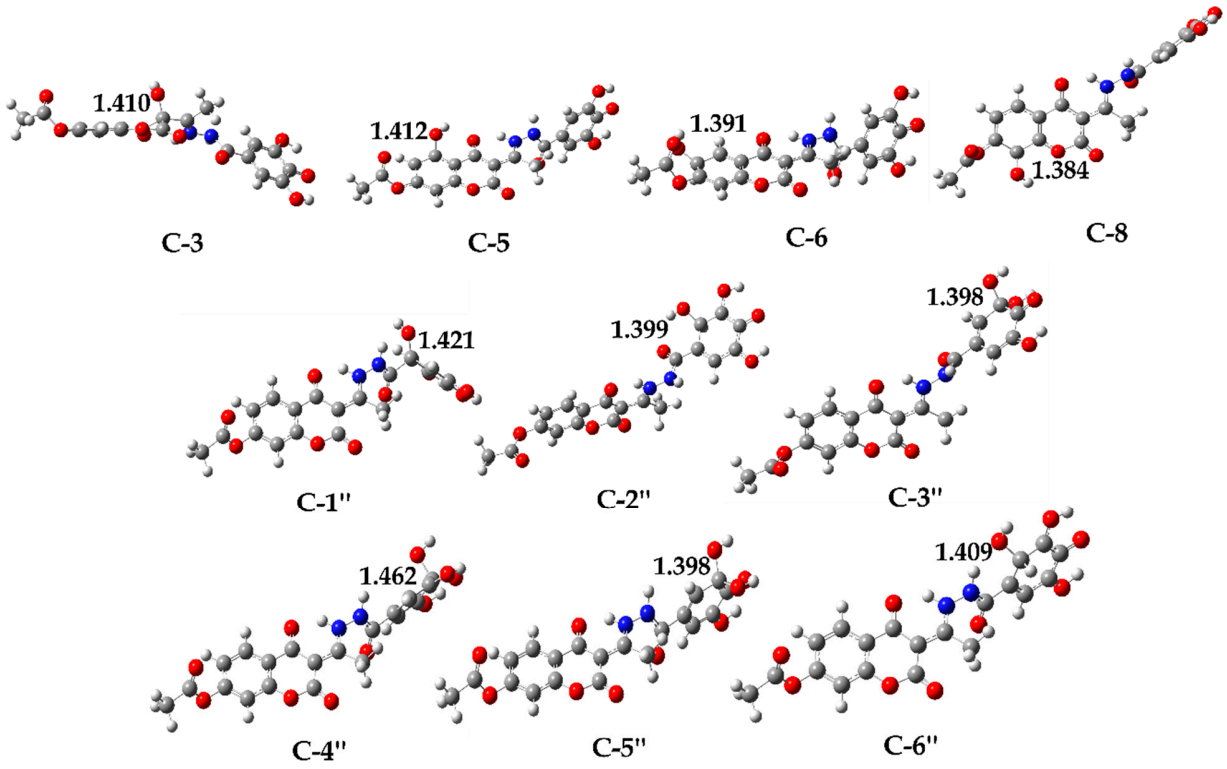

Figure S10. Optimized geometries of adducts with characteristic intramolecular distances (Å) formed between $\mathbf{H_3A^{\bullet}}$ of compound **2** and $HO^{\bullet}$

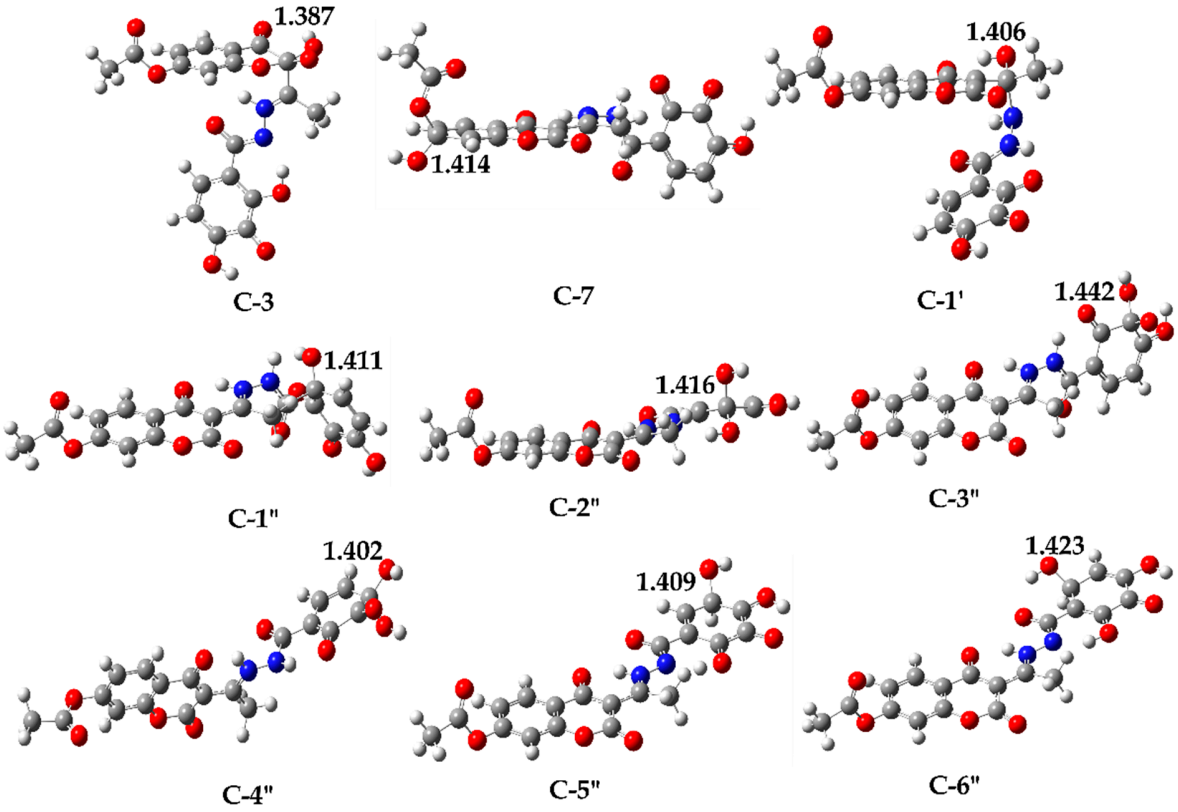

Figure S11. Optimized geometries of adducts with characteristic intramolecular distances (Å) formed between $\mathbf{H_3A^{\bullet-}}$ of compound **1** and $HO^{\bullet}$

Table S3. Estimated values of kinetic parameters: activation energy (ΔG_a, kJ mol^{-1}), rate constants of the bimolecular chemical reactions (M^{-1}s^{-1}) between the investigated compounds and HO$^{\bullet}$ estimated by the Transition State Theory (k_{TST}).

HAT/PCET				
1/2	**1 (H_4A)**		**2 (H_4A)**	
Position	ΔG_a^{HAT}	k_{TST}^{HAT}	ΔG_a^{HAT}	k_{TST}^{HAT}
2"-OH/3"-OH	58	9.53×10^{3}	59	6.79×10^{3}
3"-OH/5"-OH	41	8.26×10^{6}		
4"-OH/4"-OH	55	6.28×10^{4}	54	6.28×10^{4}
Position	**RAF**			
	1 (H_4A)		**2 (H_4A)**	
	ΔG_a^{RAF}	k_{TST}^{RAF}	ΔG_a^{RAF}	k_{TST}^{RAF}
C-3	38	3.29×10^{7}	48	6.19×10^{5}
C-5	51	1.88×10^{5}	56	2.72×10^{4}
C-6	38	3.26×10^{7}	45	2.13×10^{6}
C-7	60	1.60×10^{3}	63	1.53×10^{3}
C-8	39	2.59×10^{7}	41	9.33×10^{6}
C-9	50	2.27×10^{5}	53	7.10×10^{4}
C-10	43	4.01×10^{6}	47	9.34×10^{5}
C-1′	42	7.23×10^{6}	45	1.80×10^{6}
C-1"	37	5.60×10^{7}	35	1.02×10^{8}
C-2"	39	2.71×10^{7}	29	1.40×10^{9}
C-3"	22	1.91×10^{10}	47	9.00×10^{5}
C-4"	38	3.17×10^{7}	29	1.53×10^{9}
C-5"	38	3.38×10^{7}	39	2.08×10^{7}
C-6"	28	2.06×10^{7}	25	6.80×10^{9}

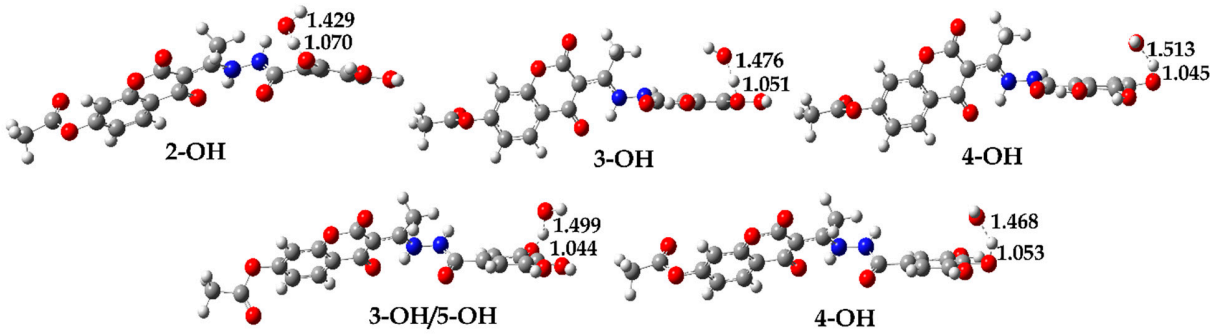

Figure S12. Optimized transition state geometries for HAT/PCET reaction pathways between neutral **H₄A** of compound **1** (top) and **2** (bottom) and HO• with characteristic intraatomic distances (Å)

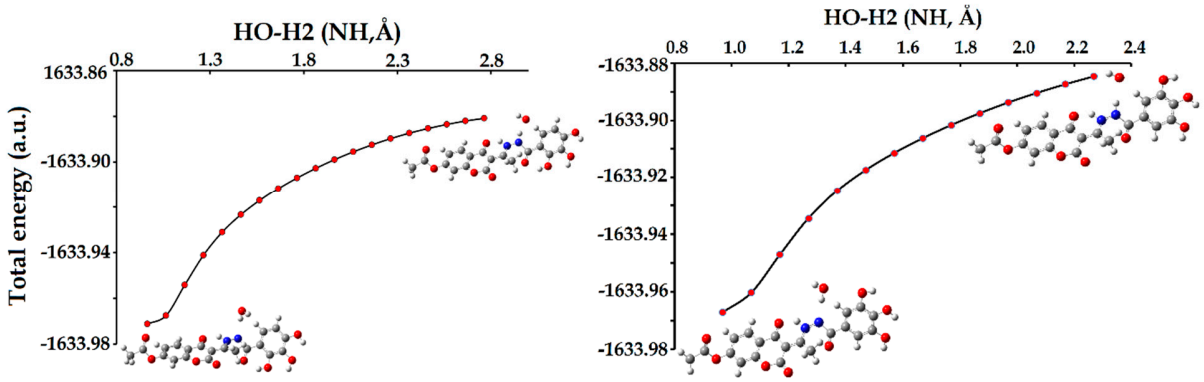

Figure S13. Dependence of the total energy (a.u.) on the HO–H2 characteristic distance (Å) for the HAT/PCET mechanism between neutral **H₄A** of compound **1** (left) and **2** (right) and HO•

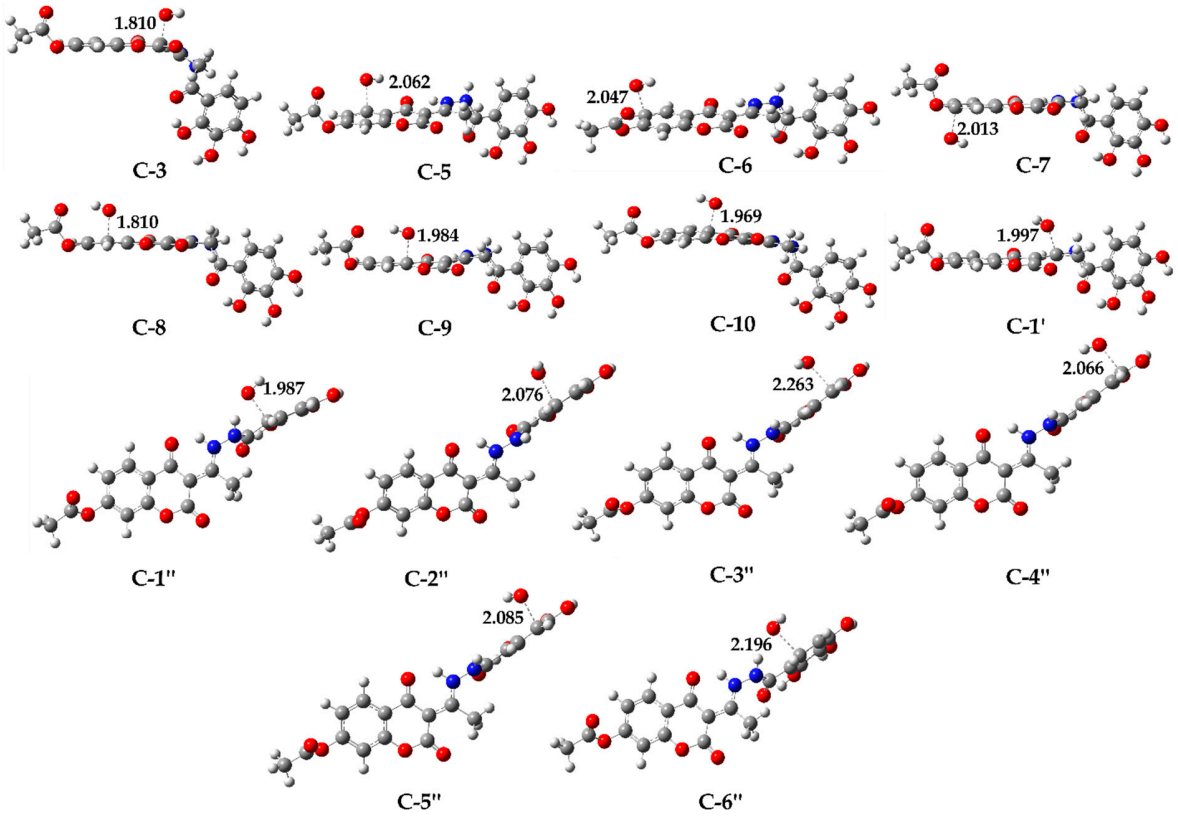

Figure S14. Optimized transition state geometries for the RAF mechanism between neutral **H_4A** of compound **1** and HO• at the M06-2X/6-311++G(d,p) level of theory with characteristic intermolecular distances (Å)

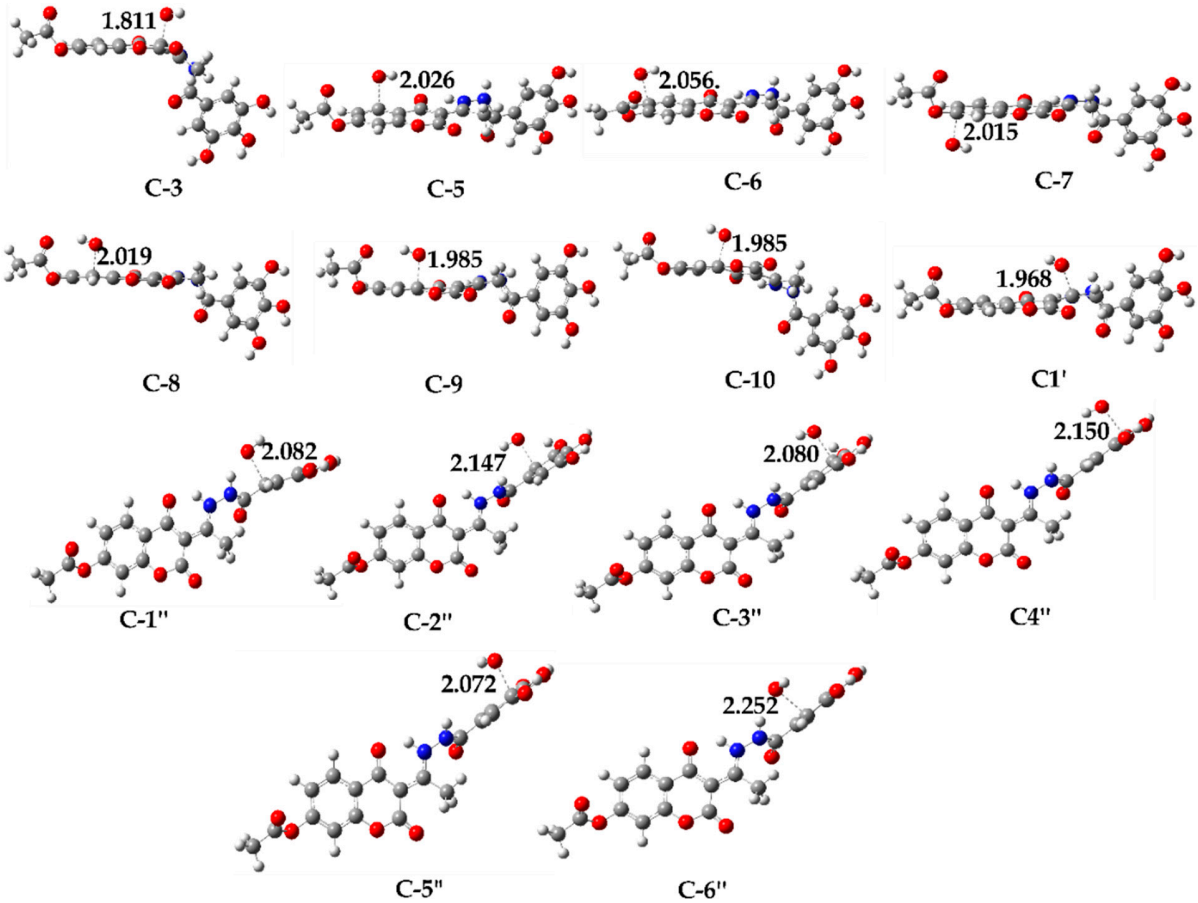

Figure S15. Optimized transition state geometries for the RAF mechanism between neutral **H_4A** of compound **2** and HO• at the M06-2X/6-311++G(d,p) level of theory with characteristic intermolecular distances (Å)

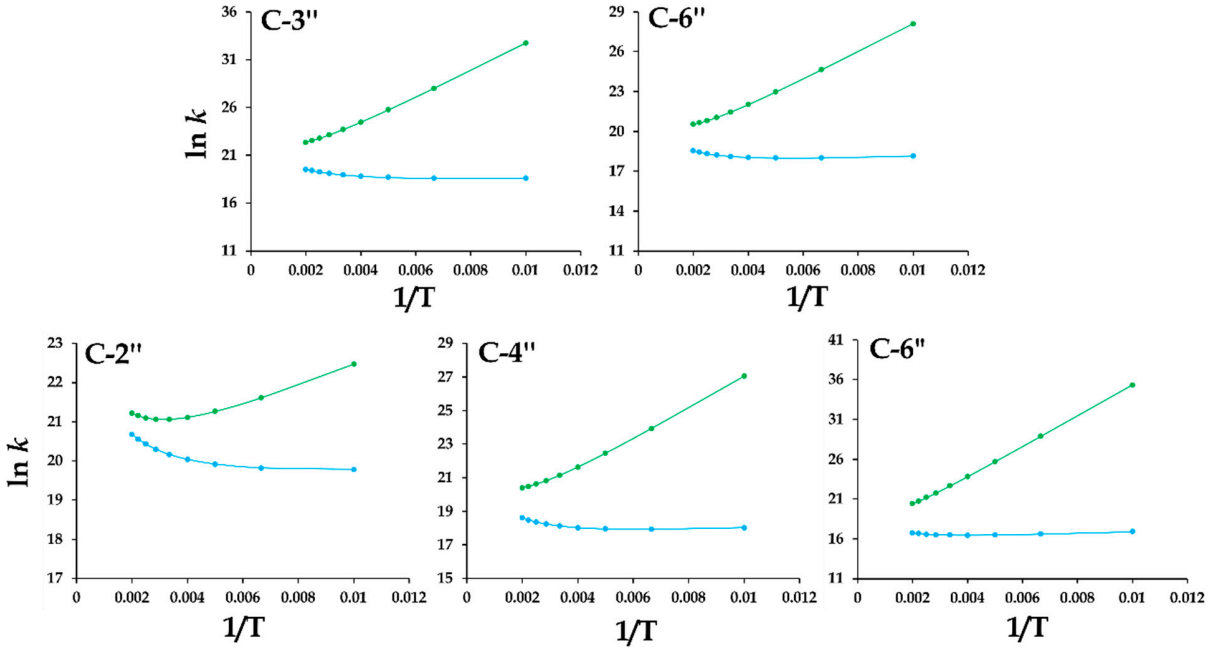

Figure S16. Graph of the dependence of lnk_{TST} (green line) and lnk_{ZCT_0} (blue line) on the reciprocal values of temperature for the RAF mechanism (**1** (top) and **2** (bottom))

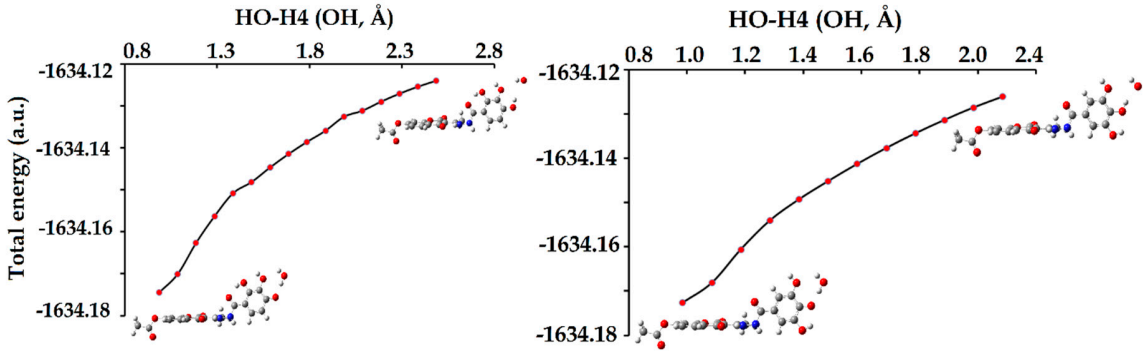

Figure S17. Dependence of the total energy (a.u.) on the HO–H4 characteristic distance (Å) for the SPL mechanism between neutral **H_4A** of compound **1** (left) and **2** (right) and HO^-

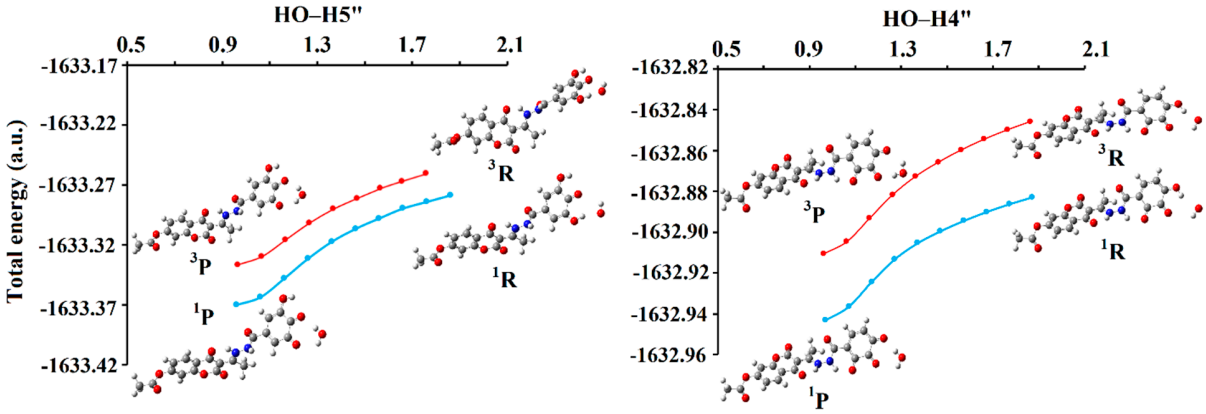

Figure S18. Energy profile for the HAT/PCET reaction pathway between **H₃A**• of compound **2** and HO• (left) as well as **H₂A**•⁻ of compound **1** and HO• (right) in the singlet (blue) and triplet (red) spin states. Interatomic distances are given in angstroms [Å]

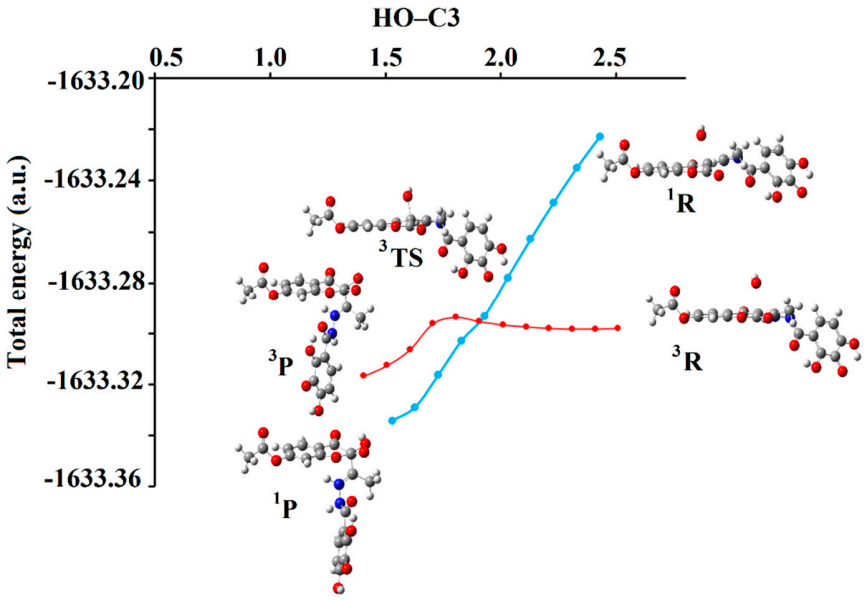

Figure S19. Energy profile for the RCF reaction path between **H₃A**• of compound **1** and HO• in the singlet (blue) and triplet (red) spin states. Interatomic distances are given in angstroms [Å]

Table S4. Estimation values of overall rate constants ($k_{overall}$), relative antiradical capacity (r^T) and branching ratios, Γ_i (%), for exergonic reaction pathways evaluated at physiological conditions, pH=7.4.

Mechanism	Position	Compound **1**			Compound **2**	
		H_4A	**H_3A^-**	**H_2A^{2-}**	**H_4A**	**H_3A^-**
HAT/PCET	**2″-OH/3″-OH**	0.0	1.6	/	0.0	0.9
	3″-OH/4″-OH	0.0	/	/	0.0	/
	4″-OH/5″-OH	0.0	1.6	0.4	0.0	0.9
	2-NH	3.1	1.6	0.4	3.7	0.9
RAF/RCF	**C-3**	0.1	22.0	5.6	0.0	12.6
	C-5	0.0			0.0	
	C-6	0.1			0.0	
	C-7	0.0			0.0	
	C-8	0.1			0.0	
	C-9	0.0			0.0	
	C-10	0.0			0.0	
	C-1′	0.0			0.0	
	C-1"	0.1			0.2	
	C-2"	0.1			1.1	
	C-3"	0.3			0.0	
	C-4"	0.1			0.1	
	C-5"	0.1			0.0	
	C-6"	0.1			0.0	
SPL/SET	***n*-OH/*n*-NH**	12.3	6.2	0.4	14.7	3.9
ET/PT	**2″-O/3″-O**	12.9	1.6	/	15.5	0.9
	3″-O/4″-O	12.2	/		15.5	/
	4″-O/5″-O	12.9	1.6	0.4	15.3	0.9
	2-N	0.2	1.6		11.3	0.9
$k_{overall}$		**3.75×10^{10}**			**4.11×10^{10}**	
r^T_{Tx}		**19.1**			**21.2**	
r^T_{GA}		**1.5**			**1.6**	